

A Moving Discontinuous Galerkin Finite Element Method with Interface Condition Enforcement for Compressible Multi- Material Flows

H. Luo*, G. Absillis* and R. Nourgaliev**
Corresponding author: hong_luo@ncsu.edu

*Department of Mechanical and Aerospace Engineering, North Carolina State University,
Raleigh, NC 27695, USA

**Lawrence Livermore National Laboratory, Livermore, CA 94550, USA

Abstract: A moving discontinuous Galerkin finite element method with interface condition enforcement (MDG-ICE) is developed for solving compressible multi-material flow problems using a mixing model, where both flow field and grid geometry are considered as independent variables and solved simultaneously. A space-time DG formulation is used to solve the conservation laws in the standard discontinuous solution space and the discrete grid geometry is solved using a variational formulation in a continuous space. The resulting over-determined system of nonlinear equations arising from the MDG-ICE formulation is solved using a self-adaptive Levenberg-Marquardt method. A number of numerical experiments for compressible material flows are conducted to assess accuracy and performance of the developed MDG-ICE method. Numerical results obtained indicate that the MDG-ICE method is able to deliver the designed order of p -convergence even for discontinuous solutions, and detect and fit all types of discontinuities and interactions of different discontinuities due to the interface condition enforcement and grid movement.

Keywords: Discontinuous Galerkin methods, Interface Conservation, Moving Grids, Compressible Multi-material Flows.

1 Introduction

The discontinuous Galerkin (DG) finite element methods [1-30] have become a popular choice to solve conservation laws with arbitrary order of accuracy. They are widely used in different computation areas including computational fluid dynamics, computational acoustics and computational magnetohydrodynamics. The discontinuous Galerkin methods have many attractive advantages like 1) its ability to achieve high-order (>2 nd) accuracy on fully unstructured grids; 2) useful mathematical properties with respect to conservation, stability and convergence; 3) its adjoint consistency to be powerful for adjoint-based optimization. In addition, the methods can also handle non-conforming elements, where the grids are allowed to have hanging nodes. Furthermore, spacetime discontinuous Galerkin methods [31-33] provide discretization of systems of conservation laws by simultaneously discretizing space and time. Like other DG methods, the spacetime DG method also offers the prospect of both arbitrary-order accuracy in space and time and adjoint consistency. However, the DG methods have a number of weaknesses that have not yet be addressed. Besides of computational cost and storage requirement, one aspect is how the properties behave in flows that are not smooth and contain discontinuous interfaces, such as material interface and shocks. Even though DG explores a set of discrete function space with discontinuous, piecewise polynomials and it can represent the discontinuous interfaces in principal, this requires that the interfaces are aligned with the grids. The stability of the DG approach may fail when misaligned grid is used. Indeed, how to control spurious oscillations in the presence of strong discontinuities has been an outstanding issue, whose mathematically sound and numerically effective solution has been an active research subject for many decades.

Moving grid methods [34-37] are a widely used approach for solving a variety of flow problems in computational fluid dynamics. In Lagrangian hydrodynamics, grids are moved to tracking contact discontinuities and material interfaces. Arbitrary Lagrangian-Eulerian (ALE) methods are widely used for moving and deforming boundary problems. In R-adaptation methods, mesh points are moved into regions of needed high resolution, which can significantly increase solution accuracy. In shock-fitting schemes, grids are moved to track shock waves.

Recently, a moving discontinuous Galerkin finite element method with interface condition enforcement, termed MDG-ICE, was formulated for compressible flows with discontinuous interfaces by Corrigan et al. [38-41], where both conservative quantities and discrete grid geometry are treated as independent variables and both conservation laws and interface conservation (IC) are solved simultaneously in the space-time domain. In the MDG-ICE formulation, a space-time DG formulation is used to solve the governing equations in the standard discontinuous solution space, and the geometry variables are determined by enforcing the interface condition in its discontinuous solution trace space. A variant of MDG-ICE [42,43] was introduced by Luo et al., where a different variational formulation is used to enforce the interface conservation. Two attractive features of the MDG-ICE method, among others, are 1) no strategies in the form of a limiter or an artificial viscosity are required to eliminate spurious oscillations in the vicinity of discontinuities and thus maintain the nonlinear stability of the DG methods, as interfaces are detected by the interface condition enforcement, and tracked by the grid movement and the interface condition; and 2) no numerical fluxes in the form of a Riemann solver have to be needed to maintain linear stability of the DG methods. Numerical results obtained indicate that the MDG-ICE methods are able to deliver the designed order of p -convergence even for discontinuous solutions, and detect and fit all types of discontinuities and interactions of different discontinuities due to the interface condition enforcement and grid movement.

The objective of the efforts presented in this work is to extend the MDG-ICE method [43] for solving compressible multi-material flow problems using a mixing model. In this MDG-ICE formulation, the compressible Euler equations along with the mass fraction equations are solved using a standard space-time DG formulation, while the geometric variables are determined by enforcing the interface conservation using a continuous variational formulation. The resulting over-determined system of nonlinear equations arising from the MDG-ICE formulation is then solved in a least-squares sense, leading to an unconstrained nonlinear least-squares problem, which is solved by a self-adaptive Levenberg-Marquardt method [44]. A number of numerical experiments for both 1D unsteady and 2D steady compressible multi-material flow problems are conducted to assess accuracy and robustness of the developed MDG-ICE method. Numerical results obtained indicate that the MDG-ICE method is able to deliver the designed optimal order of convergence even for discontinuous solutions and solutions with singularities, detect all types of discontinuities via interface conservation enforcement, and satisfy the compressible multi-material Euler equations and the interface conservation via grid movement and management. The superior accuracy of the MDG-ICE method is attributed to the enforcement of the interface conservation, while the robustness of the MDG-ICE method is attributed to the renunciation of using an upwind flux function to achieve the linear stability and limiters/ENO/WENO/Artificial viscosity strategies to achieve the nonlinear stability. The remainder of this paper is organized as follows. The governing equations are described in Section 2. The developed MDG-ICE method is presented in Section 3. Numerical experiments are reported in Section 4. Concluding remarks and future work are given in Section 5.

2 Governing Equations

The compressible Euler equations governing unsteady inviscid compressible multi-material flows using a mixing model can be expressed in conservative form as

$$\frac{\partial \mathbf{U}}{\partial t} + \frac{\partial \mathbf{f}_i(\mathbf{U})}{\partial x_i} = 0, \quad (2.1)$$

where the summation convention is used. The conservative variable vector \mathbf{U} , and inviscid flux vector \mathbf{f}_i are defined by

$$\mathbf{U} = \begin{pmatrix} \rho \\ \rho u_i \\ \rho e \\ \rho Y_{s-1} \end{pmatrix} \quad \mathbf{f}_i = \begin{pmatrix} \rho u_i \\ \rho u_j u_i + p \delta_{ij} \\ u_i(\rho e + p) \\ \rho u_i Y_{s-1} \end{pmatrix} \quad (2.2)$$

Here ρ , p , and e denote the density, pressure, and specific total energy of the mixing fluid, respectively, s is the number of materials, Y_s is the mass fraction for the material s , and u_i is the velocity of the flow in the coordinate direction x_i . The pressure is determined by the equation of state

$$p = (\gamma - 1)\rho \left(e - \frac{1}{2} u_i u_i \right) \quad (2.3)$$

which is valid for calorically perfect gases. The ratio of specific heats for the mixture γ in Eq. (2.3) is determined by

$$\gamma = \sum_{i=1}^s Y_i \gamma_i, \quad (2.4)$$

where γ_i is the ratio of the specific heats for the material i . Note that only $s-1$ mass fraction equations are solved and the mass fraction for the s material is obtained by the compatibility condition,

$$\sum_{i=1}^s Y_i = 1 \quad (2.5)$$

We are mainly interested in solving the 1D unsteady and 2D steady compressible multi-material Euler equations. For the 1D unsteady compressible multi-material Euler equations, Eq. (2.1) can be written as a 2D problem in the $x-t$ domain, $\Omega(x,t)$

$$\frac{\partial \mathbf{F}_x}{\partial x} + \frac{\partial \mathbf{F}_t}{\partial t} = 0, \quad (2.6)$$

where the two independent variables are time t and x -coordinate x , and the x - and t -components of the flux vector \mathbf{F} are

$$\mathbf{F}_x = \mathbf{f} = \begin{pmatrix} \rho u \\ \rho u^2 + p \\ u(\rho e + p) \\ \rho u Y_{s-1} \end{pmatrix}, \text{ and } \mathbf{F}_t = \mathbf{U} = \begin{pmatrix} \rho \\ \rho u \\ \rho e \\ \rho u Y_{s-1} \end{pmatrix}, \quad (2.7)$$

with u as the velocity in the x -direction. For the 2D steady-state compressible Euler equations, Eq. (2.1) can be expressed as a 2D problem in the $x-y$ domain, $\Omega(x,y)$

$$\frac{\partial \mathbf{F}_x}{\partial x} + \frac{\partial \mathbf{F}_y}{\partial y} = 0, \quad (2.8)$$

where the two independent variables are x - and y -coordinates (x,y) , and the x - and y -components of the flux vector \mathbf{F} are

$$\mathbf{F}_x = \mathbf{f}_x = \begin{pmatrix} \rho u \\ \rho u^2 + p \\ \rho u v \\ u(\rho e + p) \\ u \rho Y_{s-1} \end{pmatrix}, \text{ and } \mathbf{F}_y = \mathbf{f}_y = \begin{pmatrix} \rho v \\ \rho v u \\ \rho v^2 + p \\ v(\rho e + p) \\ v \rho Y_{s-1} \end{pmatrix}, \quad (2.9)$$

with u and v are the velocity components of the flow in the x -, and y -direction, respectively.

3 Moving Discontinuous Galerkin Method with Interface Conservation Enhancement

3.1 Space-time discontinuous Galerkin formulation

In the space-time discontinuous Galerkin formulation [31-33], the space and time are treated indistinguishably. A time-dependent problem can simply be regarded as a steady problem on a $d+1$ -dimensional space-time mesh in a finite time interval $[0, T]$, where $d = 1, 2, 3$ is the spatial dimension and $+1$ is the time dimension. Without loss of generality and for the sake of clarity, we present the space-time DG formulation for 1D unsteady multi-material Euler equations (2.7). We first introduce some notations. We assume that the space-time domain $\Omega(x, t)$ is subdivided into a collection of non-overlapping elements $\Omega_e(x, t)$. We use $\Gamma_e(x, t)$ to denote the boundary of Ω_e and \mathbf{n} the unit outward normal vector to Γ_e . We introduce the following broken Sobolev space \mathbf{V}_h^p

$$\mathbf{V}_h^p = \{v_h \in [L_2(\Omega)]^m : v_h|_{\Omega_e} \in [\mathbf{V}_p]^m \forall \Omega_e \in \Omega\}, \quad (3.1)$$

which consists of discontinuous vector-valued polynomial functions of degree p , and where m is the dimension of the unknown vector \mathbf{U} and \mathbf{V}_p is the space of all polynomials of degree $\leq p$. To formulate the discontinuous Galerkin method, we introduce the following weak formulation, which is obtained by multiplying the above conservation laws (2.6) by a test function w_h , integrating over an element Ω_e , and then performing an integration by parts,

$$\left\{ \begin{array}{l} \text{Find } \mathbf{U}_h \in \mathbf{V}_h^p \text{ such that} \\ - \int_{\Omega_e} \mathbf{F}(\mathbf{U}_h) \cdot \nabla w_h \, d\Omega + \int_{\Gamma_e} \mathbf{F}(\mathbf{U}_h) \cdot \mathbf{n} w_h \, d\Gamma = 0, \quad \forall w_h \in \mathbf{V}_h^p \end{array} \right. \quad (3.2)$$

where \mathbf{U}_h and w_h are represented by piecewise-polynomial functions of degree p , which are discontinuous between cell interfaces. Assume that B_i is the basis of polynomial functions of degree p , Eq. (3.2) is then equivalent to the following system of N nonlinear equations,

$$\left\{ \begin{array}{l} \text{Find } \mathbf{U}_h \in \mathbf{V}_h^p \text{ such that} \\ - \int_{\Omega_e} \mathbf{F}(\mathbf{U}_h) \cdot \nabla B_i \, d\Omega + \int_{\Gamma_e} \mathbf{F}(\mathbf{U}_h) \cdot \mathbf{n} B_i \, d\Gamma = 0, \quad 1 \leq i \leq N \end{array} \right. \quad (3.3)$$

where N is the dimension of the polynomial function space. Since the numerical solution \mathbf{U}_h is discontinuous between element interfaces, the interface space-time fluxes are not uniquely defined, and need to be computed carefully from the consideration of stability. This scheme is called the discontinuous Galerkin method of degree p , or in short notation DG(P) method. By simply increasing the degree p of the polynomials, the DG methods of corresponding higher order are obtained. The domain and boundary integrals in Eq. (3.3) are calculated using Gauss quadrature formulas. The number of quadrature points used is chosen to integrate exactly polynomials of order of $2p$ and $2p+1$ for the volume and surface inner products in the reference element. A numerical polynomial solution \mathbf{U}_h in each element is expressed using a standard finite element basis as following

$$\mathbf{U}_h = \sum_{i=1}^N \mathbf{U}_i B_i(x, t) \quad (3.4)$$

where B_i are a set of polynomial basis functions and \mathbf{U}_i are the unknown coefficients to be determined. Our implementation of the DG method is designed to be rather general to allow any types of the basis functions. For all the examples presented in this manuscript, Legendre and Lagrange polynomial basis functions are used to represent a DG solution for quadrilateral and triangular elements, respectively. The space-time DG formulation inherits all features of the standard DG formulation, and in addition allows uniform or different order of accuracy in space and time, as the time and space are treated in the same way. The space-time DG formulation is especially attractive for

the moving/deforming boundary problems, as the geometric conservation law is naturally satisfied. Furthermore, the issue of conservative interpolation does not exist when a remeshing occurs or the topology of a mesh is changed.

3.2 Moving discontinuous Galerkin-Interface Conservation Enhancement Formulation

Traditionally, the governing equations for the conservation laws are only solved on elements Ω_e (computational cells) as described in the previous sub-section. Similarly, the conservation laws should be enforced on element interfaces Γ_e as required by the physics.

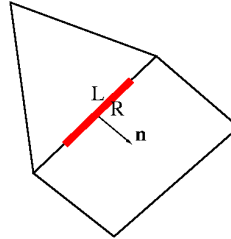


Figure 1. Illustration of a zero-thickness control volume on an interface

Applying the conservation laws on a zero-thickness control volume along an interface Γ_e as shown in red in Figure 1 leads to the following interface condition or jump condition for the flux function across the interface

$$\mathbf{F}(\mathbf{U}_h^R) \cdot \mathbf{n} - \mathbf{F}(\mathbf{U}_h^L) \cdot \mathbf{n} = \mathbf{0} \Rightarrow [\mathbf{F}(\mathbf{U}_h) \cdot \mathbf{n}] = 0, \quad (3.5)$$

where \mathbf{U}_h^R and \mathbf{U}_h^L are the conservative variable vector on the interface from the left and right elements respectively and the bracket is the so-called the jump operator. This is the so-called interface condition, which is also termed the transmission condition in the hybridized DG [45] or embedded DG [46] formulation. The interface conservation is never considered in all shock-capturing based schemes, because 1) it is automatically satisfied for smooth flows, as long as the flows are fully resolved, which can always be achieved by using high mesh resolution; 2) it can never be satisfied for flows with discontinuities by simply increasingly refined meshes, unless the discontinuities are aligned with mesh interfaces. In other words, the interface conservation can only be achieved, if and only if the mesh interfaces are aligned with discontinuities. Recognizing the importance of the interface conservation enforcement and the necessity of a mesh movement to enforce the interface conservation, the main idea behind the MDG-ICE method is to treat the discrete geometry as an independent variable, which is determined by solving and enforcing the interface conservation explicitly. Therefore, the MDG-ICE formulation is characterized by treating both flow field and discrete geometry as independent variables, and by solving the conservation laws on both elements and element interfaces simultaneously in the space-time domain. In the MDG-ICE method, discontinuous interfaces are not explicitly tracked, but rather solved and obtained implicitly as a result of the interface conservation enforcement. Furthermore, what the MDG-ICE method offers is more than detecting and fitting discontinuities, which can also be achieved by other discontinuity fitting methods. By solving the conservation laws on interfaces, a continuous solution with a discontinuous derivative, such as the head and tail of a rarefaction wave, can be exactly resolved by the MDG method as demonstrated in next section, which cannot be obtained by any other discontinuity tracking methods.

In this work, meshes are set uniform in time, i.e., cannot move in the t -direction. Furthermore, the geometric variables are determined by enforcing the interface conservation using a continuous variational formulation as follows,

$$\int_{\Gamma_e} [\mathbf{F}(u_h) \cdot \mathbf{n}] w_h = 0, \quad (3.6)$$

where w_h is a test function in the continuous solution trace space. In our implementation, Lagrange

basis functions are used to represent the test function space. The derivation of discrete equations for the interface condition is similar to the approach used in the so-called embedded DG method [46]. Figure 2 illustrates the dimension of the test function space for the interface condition in the case of a CG(P1) approximation. In this case, the number of nonlinear equations obtained from Eq. (3.6) is $n_{\text{points}} \times n_{\text{equations}}$, i.e., the number of red dots in Figure 2. The number of the geometric variables is only n_{points} , i.e., the x -coordinate of the grid vertices, as the mesh cannot move in the t -direction. This formulation always leads to an over-determined system of equations for a system of conservation laws and a determined system of equations in the case of a scalar equation. Since meshes are uniform in time, the interface condition does not need to be enforced on the faces that separate the time slabs, i.e., all horizontal faces as shown in Figure 2. In this case, fluxes on these faces in Eq. (3.3) are computed in a naturally upwind manner, as the information can only be propagated from the past to the future according to the causality principle.

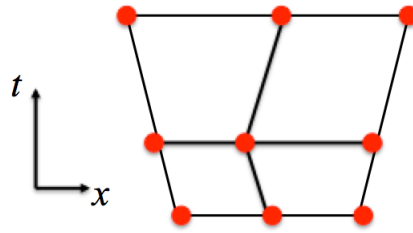


Figure 2. Illustration for the dimension of the test function space for the interface condition in the case of a CG(Q1) approximation

In our implementation, one element in time with a uniform time-step size is used, which leads to the traditional space-time DG formulation [31-33] normally described on one single space-time slab $[t_n, t_{n+1}]$ as shown in Figure 3. Our justifications of using this MDG-ICE formulation are the following: Firstly, the size of the resultant system of nonlinear equations is significantly reduced. For the DG(Q1) approximation, the number of unknown flow variables is $n_{\text{degrees}} \times n_{\text{equations}} \times n_{\text{elements}}$, while the number of geometric variables is $n_{\text{points}}/2$, i.e., the number of the grid points at time step $n+1$, as illustrated in Figure 3, where n_{degrees} designates the number of degrees of freedom in DG(P) approximation (3 for DG(P1) and 4 for DG(Q1) in general). Thus, an over-determined system of nonlinear equations for $(n_{\text{degrees}} \times n_{\text{equations}} \times n_{\text{elements}} + n_{\text{points}}/2)$ solution unknowns needs to be solved at each time step. Secondly, the implementation of the MDG method for the 3D unsteady problems becomes easy and straightforward. Otherwise, one would need to work in 4D space, which can be challenging and intimidating. Thirdly, this MDG-ICE formulation advances solutions using one cell in time and with a uniform time-step size, leading to a time-marching-like method, and consequently is easy to understand, analyze, implement, and solve.

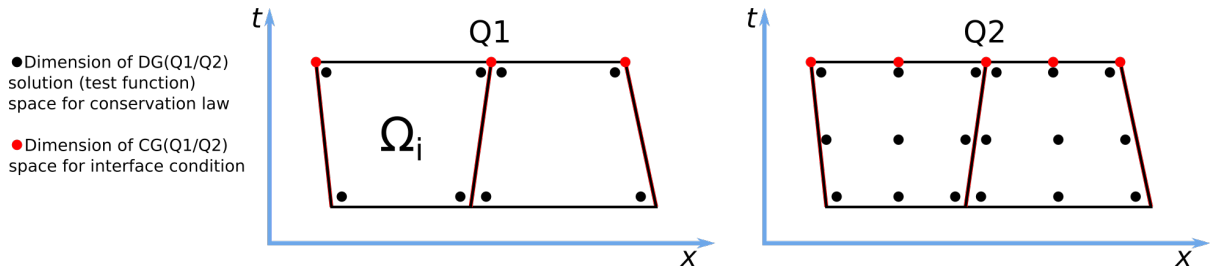


Figure 3. Illustration for the dimension of the DG(Q1/Q2) solution for conservation law and the dimension of CG(Q1/Q2) for interface condition

3.3 Numerical space-time fluxes

Since the numerical solution \mathbf{U}_h is discontinuous between element interfaces, the interface space-time

fluxes in the surface integral in Eq. (3.3) are not uniquely defined, and therefore need to be computed carefully for the consideration of consistency and stability. In the standard discontinuous Galerkin and space-time discontinuous Galerkin formulation, the flux function is replaced by a common numerical flux based on an exact or approximate Riemann solution, which is absolutely required to maintain the stability. However, in the MDG-ICE formulation, the interface space-time fluxes are uniquely defined by the enforcement of interface condition Eq. (3.5), which indicates

$$\mathbf{F}(\mathbf{U}_h^L) \cdot \mathbf{n} = \mathbf{F}(\mathbf{U}_h^R) \cdot \mathbf{n}. \quad (3.7)$$

Therefore, the flux function is not substituted by a common numerical flux function and instead the element interior flux is retained. This means that the information exchange between two neighboring cells, i.e., the global coupling, is only achieved through the enforcement of the interface condition. Instead of using the separate flux function, a common flux function as the average of the left and right flux functions

$$\mathbf{F}(\mathbf{U}_h) \cdot \mathbf{n} = \frac{1}{2}(\mathbf{F}(\mathbf{U}_h^L) \cdot \mathbf{n} + \mathbf{F}(\mathbf{U}_h^R) \cdot \mathbf{n}) \quad (3.8)$$

is used in our MDG-ICE formulation in order to enhance the stability and coupling for under-resolved flows. This simple average flux function satisfies the so-called consistency requirement for the numerical fluxes in the MDG-ICE formulation, i.e., Eq. (3.8) and is found to enhance the stability of the MDG-ICE method. It should be emphasized that the MDG-ICE formulation does not need an upwind flux function from a Riemann solution, as solving the conservation laws on interfaces enforces the interface conservation. In fact, how to extend an upwind flux to the space-time DG formulation, that satisfies the consistency requirement (3.7), is unclear and remains an open problem. On the other hand in the steady-state MDG-ICE formulation, most of the well known upwind flux functions can be directly.

3.4 Solving the nonlinear least-squares problem

As can be seen, the MDG-ICE formulation leads to an over-determined system of nonlinear equations that needs to be solved at each time step or more precisely for one space-time slab

$$\mathbf{R}(\mathbf{U}) = \mathbf{0}, \quad (3.9)$$

where \mathbf{U} is the unknown solution vector, which includes both flow variables \mathbf{U}_h and geometric variables \mathbf{x} ,

$$\mathbf{U} = \begin{pmatrix} \mathbf{U}_h \\ \mathbf{x} \end{pmatrix} \quad (3.10)$$

and \mathbf{R} represents the nonlinear residual function, which includes both residuals for the conservation laws \mathbf{R}_{cl} from Eq. (3.3) and interface conservation \mathbf{R}_{ic} from Eq. (3.6),

$$\mathbf{R} = \begin{pmatrix} \mathbf{R}_{cl} \\ \mathbf{R}_{ic} \end{pmatrix} \quad (3.11)$$

Let the dimension of the solution vector \mathbf{U} be n and the dimension of the nonlinear residual vector \mathbf{R} be m . Since $m > n$, the over-determined system of nonlinear equations (3.9) is solved in a least-squares sense

$$\min \frac{1}{2} \sum_{i=1}^m \mathbf{R}_i^2 = \frac{1}{2} \|\mathbf{R}\|^2 \quad (3.12)$$

A number of numerical methods exist to solve the non-linear optimization problem (3.12), including steepest decent method, Newton method, Gauss-Newton method, Newton method, and Levenberg-Marquardt method [47-50]. In the current work, a self-adaptive Levenberg-Marquardt method [44] is used for solving the unconstrained minimization problem (3.12).

4 Numerical Examples

The developed MDG-ICE method is used to solve a variety of compressible multi-material flow problems. A few examples are presented here to demonstrate the accuracy, robustness, and ability of the MDG-ICE method for both 1D unsteady and 2D steady compressible multi-material flow problems. Since there is no confusion, we will use abbreviation MDG-ICE and MDG interchangeably.

A. Multi-material Sod shock tube problem

The classic multi-material Sod shock tube problem is one of the most widely used test cases, since it represents an exact solution to the full system of one-dimensional unsteady multi-material Euler equations. The exact solution contains simultaneously a shock wave, a contact discontinuity, and a rarefaction wave, which all emanate from one singularity point at $t=0$. This constitutes a particularly interesting and challenging problem for the space-time formulation where the singularity point exists and for the discontinuity tracking methods where different types of unknown interfaces exist. This example is chosen to assess (1) the ability of the MDG-ICE method to resolve singular points, and detect and fit discontinuities, (2) the robustness of the MDG-ICE method on highly distorted grids, and (3) the order of p -convergence of the MDG-ICE method for discontinuous solutions. The initial conditions in the computation are the following:

$$(\rho, v, p, \gamma)(x, t = 0) = \begin{cases} (1, 0, 1, 1.667), & -0.5 \leq x < 0, \\ (0.125, 0, 0.1, 1.2) & 0 < x \leq 0.5 \end{cases}$$

Computation is performed on a single space-time slab $\Omega(x,t)=(-0.5,0.5)\times(0,0.2)$ with 8 quadrilateral elements where the left 7 elements are initiated with the piecewise left constant state and the right one element is initiated with the piecewise constant right state. Figure 3 shows the initial grid used in this numerical experiments along with the initial density fields. Six middle cells are degenerated at the origin $(0,0)$, which are necessary to resolve the singularity point accurately and adequately. Numerical solutions are computed using the MDG(P1), MDG(P2), and MDG(P3) methods. Figure 4 shows a comparison of the density, pressure, and velocity profiles at $t=0.2$ between the exact solution and the computed MDG(P1) and MDG(P2) solutions, respectively. The MDG(P3) solutions are compared with the analytical solution in Figure 5, where a comparison of the mass fraction profile at $t=0.2$ for MDG(P1), MDG(P2), and MDG(P3) solutions is also provided. The MDG (P1) solutions are represented using a two-point connecting straight line on each element, while the MDG(P2) and MDG(P3) solutions are represented using a three-point connecting line on each element. As expected, the MDG(P1) solution is under-resolved for the rarefaction wave, because of the coarse grid used in this test case, although both shock and contact discontinuity are accurately fitted. Both MDG(P2) and MDG(P3) solutions are able to capture and fit both shock and contact as true discontinuities at the correct locations. In addition, the position of the head and tail of the refraction wave, where a derivative discontinuity exists, is virtually resolved exactly by the MDG(P2) and MDG(P3) solutions. This superior accuracy of the MDG method should be attributed to the fact that the interface conservation is solved and enforced explicitly, as all discontinuity tracking and fitting methods are not purposely designed to accurately fit continuous solutions where their derivatives are discontinuous. A p -refinement study for this problem is conducted to numerically obtain quantitative measurement of the absolute errors and order of p -convergence for the MDG method. The following L_2 function norm in the space-time domain $\Omega(x,t)$ is used to measure the error of the MDG method

$$\|u_c - u_e\|_{L_2} = \sqrt{\int_{\Omega(x,t)} (u_c - u_e)^2 d\Omega}$$

where u_c and u_e are the computed and exact solutions, respectively. L_2 function norm of the error function is plotted in Figure 6 against the inverse of the square root of the number of degrees of freedom on a log-log scale. One can clearly observe that the MDG method exhibits an exponential rate of convergence for the p -type refinement, which is reflected by the downward curving line instead of a straight line for the h -refinement. This example demonstrates some of the most attractive features of the MDG method due to the interface conservation enforcement: being able to detect and fit different types of discontinuities automatically without resorting to specialized logics specific to each type and achieving the formal rate of p -convergence even for discontinuous solutions and solutions with singularities, that no other numerical methods can to the best of our knowledge. Solving and enforcing the conservation laws on interfaces enable the MDG-ICE method to not only detect and fit the contact discontinuity and shock wave but also exactly resolve the head and tail of the rarefaction wave, where the solutions are continuous but their derivatives are discontinuous.

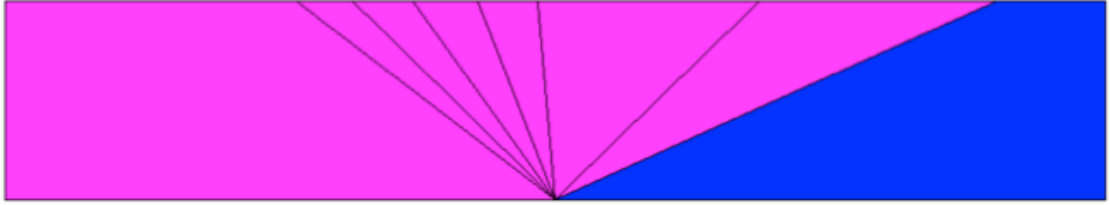


Figure 3. Initial space-time grids and density fields on $\Omega=(-0.5,0.5)\times(0,0.2)$ for multi-material Sod shock tube problem

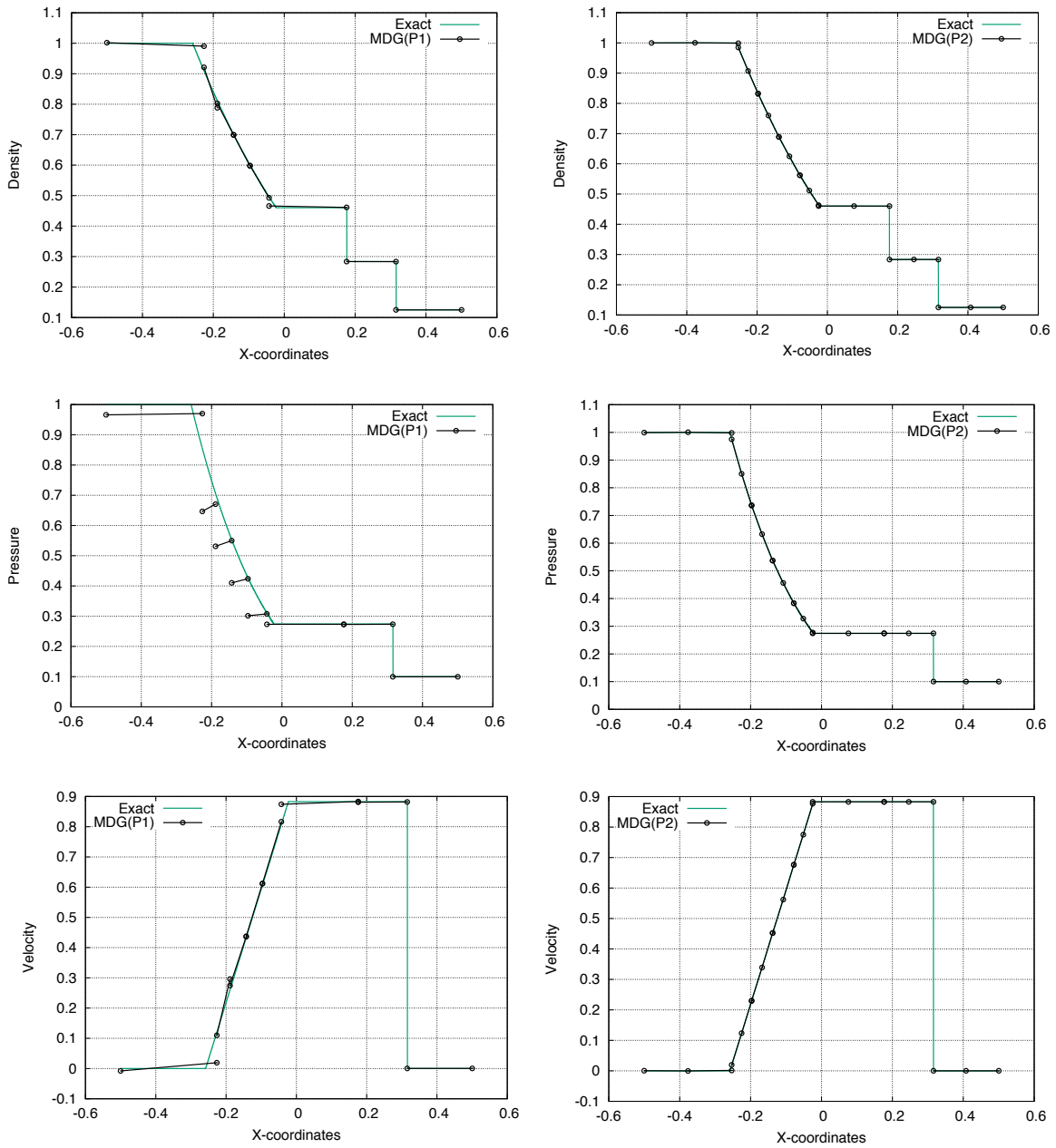


Figure 4. Comparison of density, pressure, and velocity at $t=0.2$ between the analytical solution and MDG(P1) (left), and the analytical solution and MDG(P2) (right) solution, respectively.

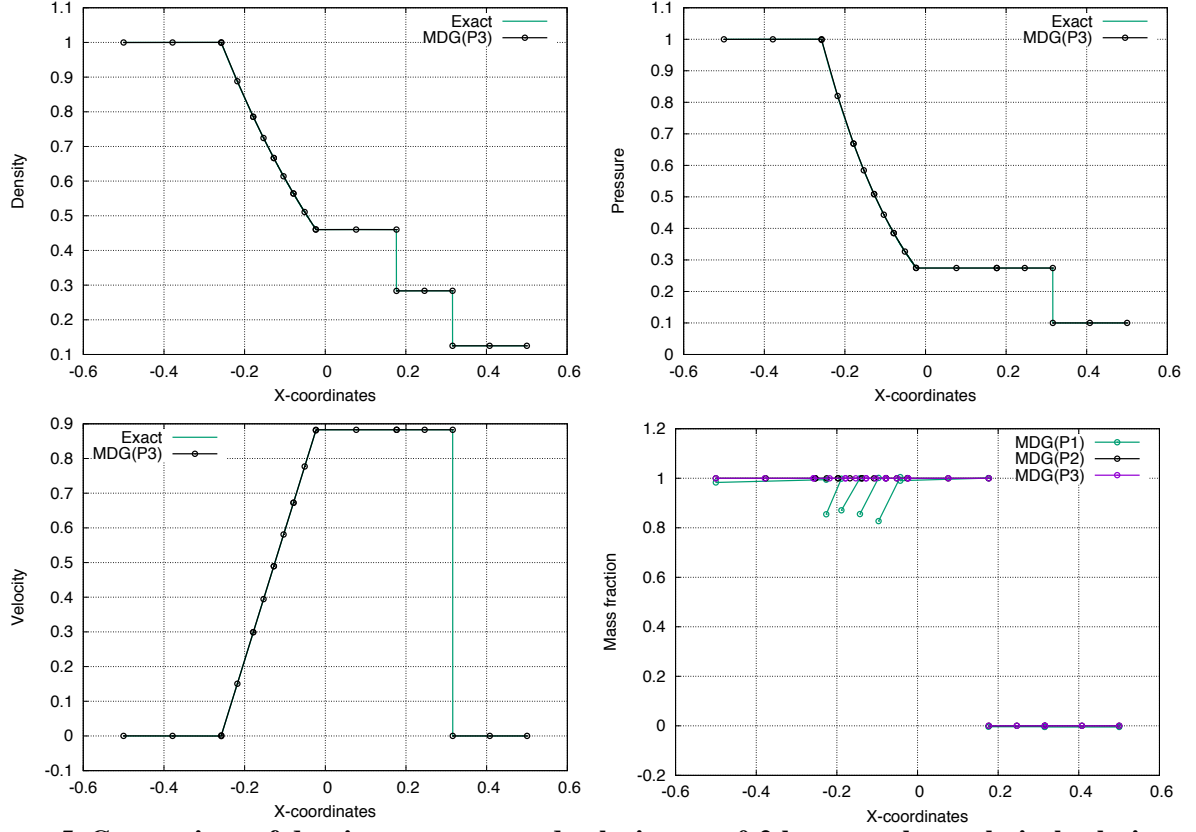


Figure 5. Comparison of density, pressure, and velocity at $t=0.2$ between the analytical solution and MDG(P3) (top and lower-left), and comparison of mass fraction profile at $t=0.2$ among MDG(P1), MDG(P2), and MDG(P3) solutions (lower-right)

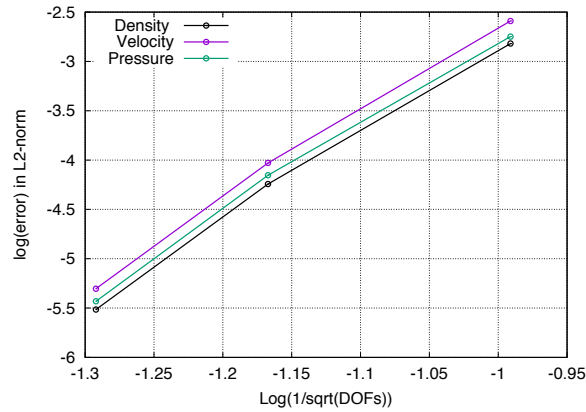


Figure 6. Convergence histories of density, velocity, and pressure for p-refinement

B. Multi-material Lax-Harden Riemann problem

This is another well-known test case for the multi-material shock tube problem. The initial conditions in the present computation are the following:

$$(\rho, v, p, \gamma)(x, t = 0) = \begin{cases} (0.445, 0.698876404, 3.52773, 1.4), & -0.5 \leq x < 0, \\ (0.5, 0, 0.571, 5/3) & 0 < x \leq 0.5 \end{cases}$$

Computation is performed using 8 quadrilateral cells on a space-time domain $\Omega = (-0.5, 0.5) \times (0, 0.15)$ where the left 7 elements are initiated with the piecewise left constant state and the right one element is initiated with the piecewise constant right state. Initial mesh and density field are shown in Figure 7. Six middle cells are degenerated at the origin $(0, 0)$, which are necessary to resolve the singularity point accurately and adequately. Numerical solutions are computed using the MDG(P1) and MDG(P2) methods. Figure 8 shows the density, pressure, and velocity profiles at $t=0.15$, comparing the exact

solution and the two computed MDG solutions, respectively. A comparison of the mass fraction profile at $t=0.2$ for the MDG(P1) and MDG(P2) solutions is provided in Figure 9. Both MDG solutions are able to fit both shock and contact as true discontinuities at the correct locations. Moreover, the position of the head and tail of the refraction wave, where a derivative discontinuity exists, is also fit moderately by the MDG(P1) solution due to lack of resolution and virtually exactly by the MDG(P2) solution. Again, one can observe that the MDG methods are able to detect and track multiple types of discontinuities automatically and implicitly.

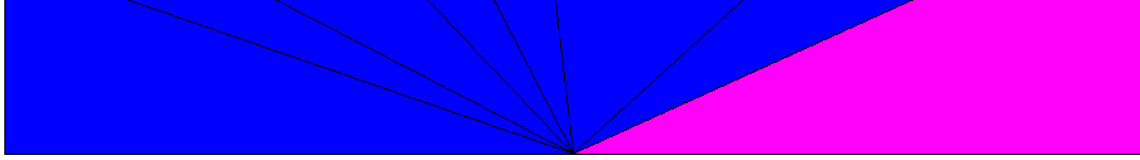


Figure 7. Initial space-time grids and density fields on $\Omega=(-0.5,0.5)\times(0,0.15)$ for multi-material Lax-Harden shock tube problem

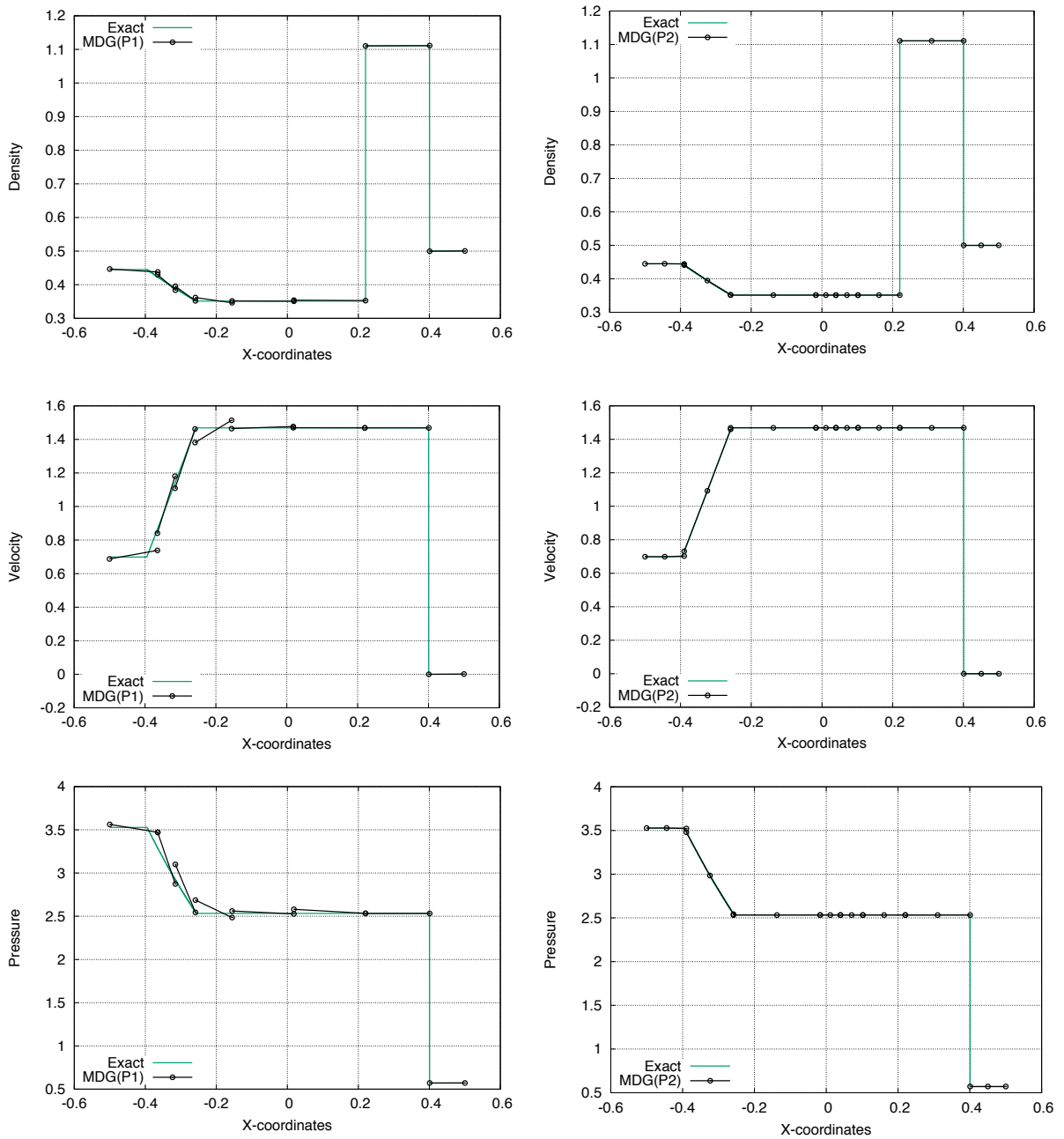


Figure 8. Comparison of density, pressure, and velocity at $t=0.15$ between the analytical solution and MDG(P1) (left), and the analytical solution and MDG(P2) (right) solution, respectively.

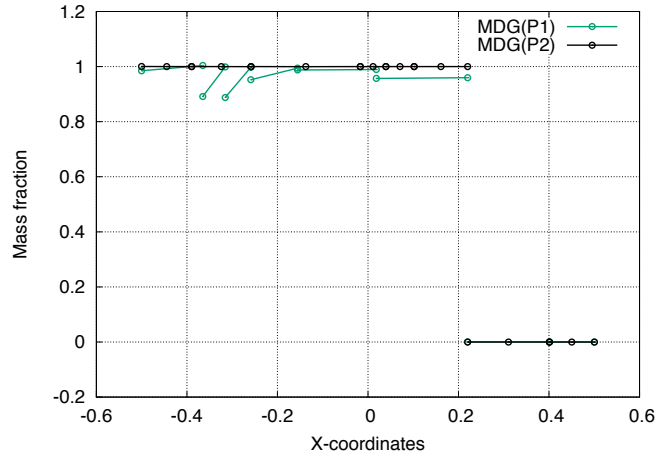


Figure 9. Comparison of the mass fraction profile between the MDG(P1) and MDG(P2) solutions at $t=0.15$.

C. Multi-material shock tube problem with a reflectionless shock

We consider a multi-material shock tube problem with a reflectionless shock. This test case is chosen to assess the ability of the MDG method for resolving singularity points, and capture and fit discontinuities on highly stretched grids. The initial conditions in the present computation are the following:

$$(\rho, v, p, \gamma)(x, t = 0) = \begin{cases} (3.2, 9.43499279, 100, 5/3), & -0.5 \leq x < -0.3, \\ (1, 0, 1, 1.2) & -0.3 < x \leq 0.5 \end{cases}$$

Computation is performed using 8 quadrilateral cells on a space-time domain $\Omega = (-0.5, 0.5) \times (0, 0.06)$ where 6 middle elements are degenerated at the origin $(-0.3, 0)$. The solutions are initiated with the piecewise left constant state and the right one element is initiated with the piecewise constant right state. Initial mesh and density field are shown in Figure 10. Numerical solution is computed using the MDG(P1) method. Figure 11 shows the density and pressure profiles at $t=0.06$, comparing the exact solution and the computed MDG(P1) solution. A comparison of the velocity profile with the exact solution along with the computed mass fraction profile at $t=0.06$ is provided in Figure 12. One can observe the ability of the MDG method for resolving singularity points, and capture and fit discontinuities.



Figure 10. Initial space-time grids and density fields on $\Omega=(-0.5,0.5) \times (0,0.06)$ for a multi-material shock tube problem with reflectionless shock

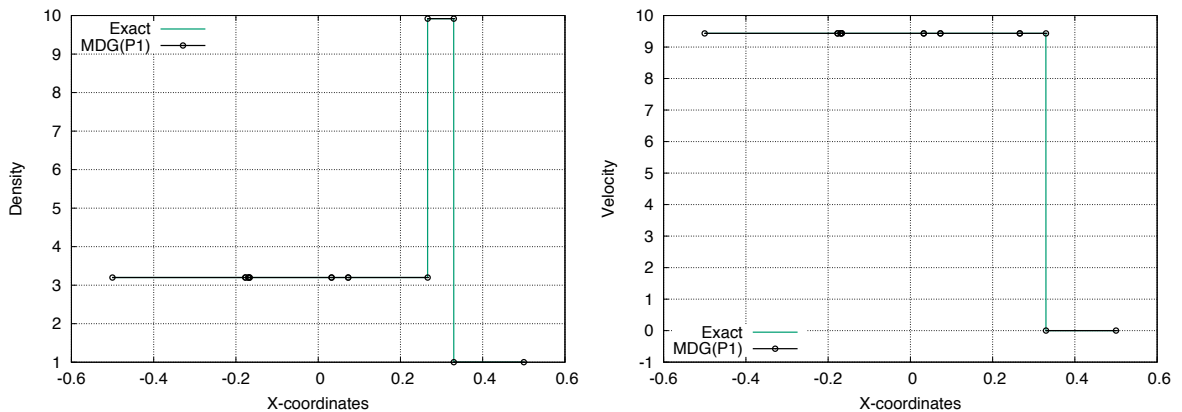


Figure 11. Comparison of the density and velocity profile at $t=0.06$ between the analytical solution and MDG(P1) solution.

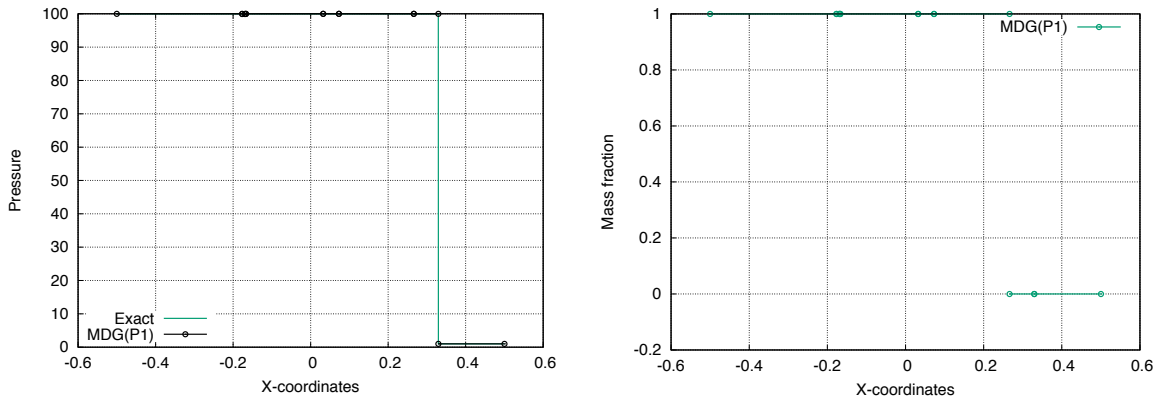


Figure 12. Comparison of the pressure profile at $t=0.06$ between the analytical solution and MDG(P1) solution (left) and the computed mass fraction profile (right) at $t=0.06$

D. Multi-material shock wave refraction problem

In this test case, we consider regular shock refraction at a carbon dioxide (CO_2)/Methane (CH_4) interface as illustrated in Fig. 13. This example is chosen to assess the ability of the MDG-ICE method for fitting discontinuities with non-trivial topology. The Mach number, pressure, and stagnation enthalpy are 2, 1, and 3, respectively. The wedge angle is 23.2° . The ratios of specific heats for CO_2 and CH_4 are 1.288 and 1.303, respectively. The mesh consists of 69 elements, 47 points, and 23 boundary faces. The solution is initialized with a uniform flow. The initial density field on the initial grid and the density field obtained by the MDG(P1) solution on the final grid are shown in Figure 14. One can observe that shock reflection, shock transmission, and refracted material interface are accurately resolved and fitted by the MDG-ICE method, clearly demonstrating the ability of the MDG-ICE method to detect, resolve, and fit discontinuities with complex topology. In fact, the MDG-ICE method is able to obtain the analytical solution for this problem due to the interface conservation enforcement, which consists of five constant states.

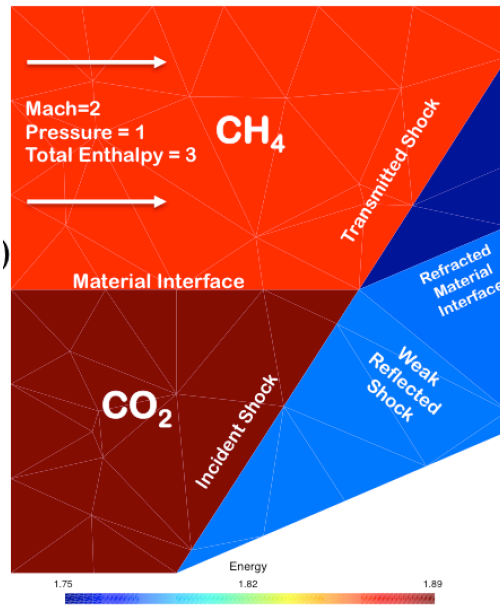


Figure 13. Illustration of the Multi-material shock wave refraction problem

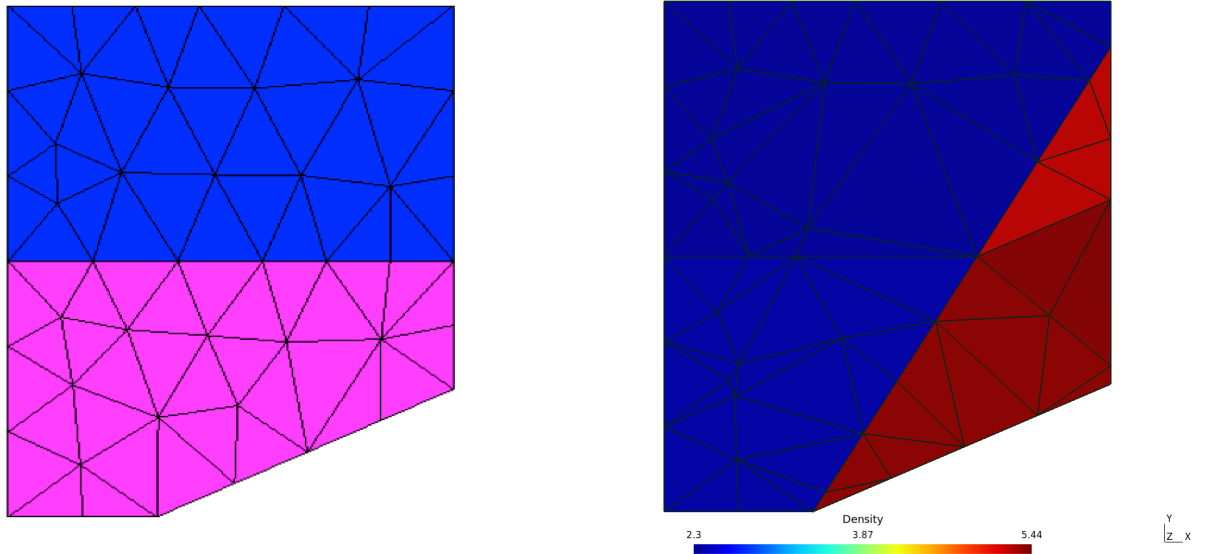


Figure 14. Initial density field on the initial grid (left) and density field obtained by the MDG(P1) solution on the final grid.

5 Conclusion and Future Work

A MDG-ICE method based on a continuous variational formulation for the interface conservation and a space-time discontinuous Galerkin formulation for the conservative laws has been developed for compressible multi-material flows using a mixing model. A number of test cases for both 1D unsteady and 2D steady compressible multi-material Euler equations have been conducted to assess the accuracy and robustness of the MDG-ICE method. The preliminary results are highly promising and encouraging, demonstrating that an exponential rate of convergence for Sod and Lax-Harden shock tube problems can be achieved, something that no other numerical methods can do to the best of our knowledge. Indeed, by recognizing the importance of the interface conservation and by enforcing the interface conservation via grid movement and grid management, the MDG-ICE method, (1) can automatically detect and fit all types of discontinuities virtually exactly and resolve accurately solutions with discontinuous derivatives, which in turn allows the MDG-ICE method to achieve the designed optimal rate of convergence even for discontinuous solutions; (2) does not have to use any exact or approximate Riemann solver-based numerical flux function to achieve stability nor does it require any strategies (limiter/ENO-WENO/artificial viscosity) to suppress spurious oscillations in the vicinity of strong discontinuities; and (3) is extremely robust in the sense that a) It can handle highly distorted and even tangled meshes with zero or even negative volumes; and b) Even negative pressure and negative density do not lead to the breakdown of a solution process. This MDG-ICE method has successfully been extended for thermal and chemical non-equilibrium reacting hypersonic flows, which will be reported in another paper. Ongoing work is focused on exploring and developing numerical algorithms to solve the resultant nonlinear least-squares problems efficiently, effectively, and reliably. The extension of the MDG-ICE method for solving viscous flow problems is also underway.

Acknowledgement

This work was performed under the auspices of the U.S. Department of Energy by Lawrence Livermore National Laboratory under Contract DE-AC52-07NA27344, and funded by the Laboratory Directed Research and Development Program at LLNL under project tracking code 19-ERD-015.

References

- [1] W.H. Reed and T.R. Hill, Triangular Mesh Methods for the Neutron Transport Equation, Los Alamos Scientific Laboratory Report, LA-UR-73-479, 1973.
- [2] B. Cockburn, S. Hou, and C. W. Shu, TVD Runge-Kutta Local Projection Discontinuous Galerkin Finite Element Method for conservation laws IV: the Multidimensional Case,

- Mathematics of Computation, Vol. 55, pp. 545-581, 1990.
- [3] B. Cockburn, and C. W. Shu, The Runge-Kutta Discontinuous Galerkin Method for conservation laws V: Multidimensional System, Journal of Computational Physics, Vol. 141, pp. 199-224, 1998.
 - [4] B. Cockburn, G. Karniadakis, and C. W. Shu, The Development of Discontinuous Galerkin Method, in Discontinuous Galerkin Methods, Theory, Computation, and Applications, edited by B. Cockburn, G.E. Karniadakis, and C. W. Shu, Lecture Notes in Computational Science and Engineering, Springer-Verlag, New York, 2000, Vol. 11 pp. 5-50, 2000.
 - [5] F. Bassi and S. Rebay, High-Order Accurate Discontinuous Finite Element Solution of the 2D Euler Equations, Journal of Computational Physics, Vol. 138, pp. 251-285, 1997.
 - [6] H. L. Atkins and C. W. Shu, Quadrature Free Implementation of Discontinuous Galerkin Method for Hyperbolic Equations, AIAA Journal, Vol. 36, No. 5, 1998.
 - [7] F. Bassi and S. Rebay, GMRES discontinuous Galerkin solution of the Compressible Navier-Stokes Equations, Discontinuous Galerkin Methods, Theory, Computation, and Applications, edited by B. Cockburn, G.E. Karniadakis, and C. W. Shu, Lecture Notes in Computational Science and Engineering, Springer-Verlag, New York, 2000, Vol. 11 pp. 197-208, 2000.
 - [8] T. C. Warburton, and G. E. Karniadakis, A Discontinuous Galerkin Method for the Viscous MHD Equations, Journal of Computational Physics, Vol. 152, pp. 608-641, 1999.
 - [9] J. S. Hesthaven and T. Warburton, Nodal Discontinuous Galerkin Methods: Algorithms, Analysis, and Applications, Texts in Applied Mathematics, Vol. 56, 2008.
 - [10] P. Rasetarinera and M. Y. Hussaini, An Efficient Implicit Discontinuous Spectral Galerkin Method, Journal of Computational Physics, Vol. 172, pp. 718-738, 2001.
 - [11] B. T. Helenbrook, D. Mavriplis, and H. L. Atkins, Analysis of p -Multigrid for Continuous and Discontinuous Finite Element Discretizations, AIAA Paper 2003-3989, 2003.
 - [12] K. J. Fidkowski, T. A. Oliver, J. Lu, and D. L. Darmofal, p -Multigrid solution of high-order discontinuous Galerkin discretizations of the compressible Navier-Stokes equations, Journal of Computational Physics, Vol. 207, No. 1, pp. 92-113, 2005.
 - [13] H. Luo, J. D. Baum, and R. Löhner, A Discontinuous Galerkin Method Using Taylor Basis for Compressible Flows on Arbitrary Grids, Journal of Computational Physics, Vol. 227, No 20, pp. 8875-8893, October 2008.
 - [14] H. Luo, J.D. Baum, and R. Löhner, On the Computation of Steady-State Compressible Flows Using a Discontinuous Galerkin Method, International Journal for Numerical Methods in Engineering, Vol. 73, No. 5, pp. 597-623, 2008.
 - [15] H. Luo, J. D. Baum, and R. Löhner, A Hermite WENO-based Limiter for Discontinuous Galerkin Method on Unstructured Grids, Journal of Computational Physics, Vol. 225, No. 1, pp. 686-713, 2007.
 - [16] H. Luo, J.D. Baum, and R. Löhner, A p -Multigrid Discontinuous Galerkin Method for the Euler Equations on Unstructured Grids, Journal of Computational Physics, Vol. 211, No. 2, pp. 767-783, 2006.
 - [17] H. Luo, J.D. Baum, and R. Löhner, Fast, p -Multigrid Discontinuous Galerkin Method for Compressible Flows at All Speeds", AIAA Journal, Vol. 46, No. 3, pp.635-652, 2008.
 - [18] M. Dumbser, D.S. Balsara, E.F. Toro, C.D. Munz. A unified framework for the construction of one-step finite volume and discontinuous Galerkin schemes on unstructured meshes. Journal of Computational Physics, 227:8209-8253, 2008.
 - [19] M. Dumbser, O. Zanotti, Very high order PNPM schemes on unstructured meshes for the resistive relativistic MHD equations. Journal of Computational Physics, 228:6991-7006, 2009.
 - [20] M. Dumbser. Arbitrary High Order PNPM Schemes on Unstructured Meshes for the Compressible Navier-Stokes Equations. Computers & Fluids, 39: 60-76. 2010.
 - [21] F. Bassi and S. Rebay, A High-Order Accurate Discontinuous Finite Element Method for the Numerical Solution of the Compressible Navier-Stokes Equations, Journal of Computational Physics, Vol. 131, pp. 267-279, 1997.
 - [22] F. Bassi and S. Rebay, Discontinuous Galerkin Solution of the Reynolds-Averaged Navier-Stokes and $k-\omega$ Turbulence Model Equations, Journal of Computational Physics, Vol. 34, pp. 507-540, 2005.
 - [23] H. Luo, L. Luo, and K. Xu, A Discontinuous Galerkin Method Based on a BGK Scheme for the Navier-Stokes Equations on Arbitrary Grids, Advances in Applied Mathematics and Mechanics, Vol. 1, No. 3, pp. 301-318, 2009.
 - [24] H. Luo, L. Luo, and R. Nourgaliev, A Reconstructed Discontinuous Galerkin Method for the Euler Equations on Arbitrary Grids, Communication in Computational Physics, Vol. 12, No. 5, pp. 1495-1519, 2012.
 - [25] H. Luo, L. Luo, R. Nourgaliev, V.A. Mousseau, and N. Dinh, A Reconstructed Discontinuous Galerkin Method for the Compressible Navier-Stokes Equations on Arbitrary Grids, Journal of Computational Physics, Vol. 229, pp. 6961-6978, 2010.

- [26]H. Luo, L. Luo, A. Ali, R. Nourgaliev, and C. Cai, A Parallel, Reconstructed Discontinuous Galerkin Method for the Compressible Flows on Arbitrary Grids, *Communication in Computational Physics*, Vol. 9, No. 2, pp. 363-389, 2011.
- [27]H. Luo, H., Y. Xia, S. Li, R. Nourgaliev, and C. Cai, A Hermite WENO Reconstruction-Based Discontinuous Galerkin Method for the Euler Equations on Tetrahedral Grids, *Journal of Computational Physics*, Vol. 231, pp. 5489-5503, 2012.
- [28]H. Luo, H., Y. Xia, S. Spiegel, R. Nourgaliev, and Z. Jiang, A Reconstructed Discontinuous Galerkin Method Based on a Hierarchical WENO Reconstruction for Compressible Flows on Tetrahedral Grids, *Journal of Computational Physics*, DOI: 10.1016/j.jcp.2012.11.026, 2012.
- [29]H. Bijl, M.H. Carpenter, V.N. Vasta, and C. A. Kennedy, Implicit Time Integration Schemes for the Unsteady Compressible Navier-Stokes Equations: Laminar Flow, *Journal of Computational Physics*, Vol. 179, pp. 313-329, 2002.
- [30]L. Wang, and D.J. Mavriplis, Implicit Solution of the Unsteady Euler Equations for High-Order Accurate Discontinuous Galerkin Discretizations. *Journal of Computational Physics*, Vol. 225, No. 2, pp. 1994–2015, 2007.
- [31]Van der Vegt, J., and Van der Ven, H., Space-time Discontinuous Galerkin Finite Element Method with Dynamic Grid Motion for Inviscid Compressible Flows: I. General Formulation, *Journal of Computational Physics*, Vol. 182, No. 2, pp. 546–585, 2002.
- [32]Klajj, C., Van der Vegt, J., and Van der Ven, H., Space-time Discontinuous Galerkin Method for the Compressible Navier-Stokes Equations, *Journal of Computational Physics*, Vol. 217, No. 2, pp. 589–611, 2006.
- [33]Lehrenfeld, C., The Nitsche XFEM-DG Space-time Method and its Implementation in Three Space Dimensions, *SIAM Journal on Scientific Computing*, Vol. 37, No. 1, pp. A245–270, 2015.
- [34]M.D. Salas, A brief history of shock-fitting. In: Springer 2011(pp.37–53).
- [35]A. Bonfiglioli, R. Paciorri, and L. Campoli, Unsteady shock fitting for unstructured grids, *International Journal for Numerical Methods in Fluids*. 2016;81(4):245–261.
- [36]D. Zou, C. Xu, H. Dong, and J. Liu, A shock-fitting technique for cell-centered finite volume methods on unstructured dynamic meshes, *Journal of Computational Physics*. 2017;345:866–882.
- [37]P. Roe and H. Nishikawa, Adaptive grid generation by minimizing residuals, *International Journal for Numerical Methods in Fluids*. Vol. 40, pp. 121–136, 2002.
- [38]A. Corrigan, A. D. Kercher, and D.A. Kessler, A Moving Discontinuous Galerkin Finite Element Method for Flows with Interfaces, *International Journal for Numerical Methods in Fluids*, DOI: 10.1002/fld.4697, 2019.
- [39]A. Corrigan, A. Kercher, D. Kessler, The moving discontinuous Galerkin method with interface condition enforcement for unsteady three-dimensional flows, in: *AIAA Scitech 2019 Forum*, AIAA-2019-0642.
- [40]A. Kercher, A. Corrigan, and D. Kessler, The Moving Discontinuous Galerkin method with Interface Condition Enforcement for viscous flows, in: *AIAA Scitech 2020 Forum*, AIAA-2020-1315.
- [41]A. Corrigan, A. Kercher, D. Kessler, and D. Wood-Thomas, Convergence of the moving discontinuous Galerkin method with interface condition enforcement in the presence of an attached curved shock, in: *AIAA Aviation 2019 Forum*, AIAA-2019-3207.
- [42]H. Luo, Y. Jiang, and R. Nourgaliev, A Moving Discontinuous Galerkin Finite Element Method for Conservation Laws, *AIAA Scitech 2020 forum*, 6-10 January 2020, Orlando, FL, AIAA-2020-1316, 2020.
- [43]H. Luo, Y. G. Absillis, and R. Nourgaliev, A Moving Discontinuous Galerkin Finite Element Method with Interface Condition Enforcement for Compressible Flows, *Journal of Computational Physics*, 445 (2021) 110618.
- [44]J. Fan and J. Pan, Convergence Properties of a Self-adaptive Levenberg-Marquardt Algorithm Under Local Error Bound Condition, *Computational Optimization and Applications*, 34, 47–6, 2006.
- [45]B. Cockburn, J. Gopalakrishnan, and R. Lazarov, Unified Hybridization of Discontinuous Galerkin, Mixed, and Continuous Galerkin Methods for Second Order Elliptic Problems, *SIAM Journal on Numerical Analysis*, Vol. 47, pp.1319-1365, 2009.
- [46]N.C. Nguyen, J. Peraire, and B. Cockburn, A class of embedded discontinuous Galerkin methods for computational fluid dynamics, *Journal of Computational Physics*, Vol. 302, pp. 674-692, 2015.
- [47]B. K. Levenberg, A method for the solution of certain nonlinear problems in least squares, *Quart. Appl. Math.* Vol. 2, pp. 164–166, 1944.
- [48]D. W. Marquardt, An algorithm for least-squares estimation of nonlinear inequalities, *SIAM J. Appl. Math.* vol. 11, pp. 431–441, 1963.

- [49]J. J. More, The Levenberg-Marquardt algorithm Implementation and theory In Lecture Notes in Mathematics No 630 Numerical Analysts, G Watson, Ed, Springer-Verlag, New York, 1978, pp 105-116.
- [50]J. E. Dennis, D. M. Gay, and R. E. Walsh, An Adaptive Nonlinear Least-Squares Algorithm, ACM Transactions on Mathematical Software, Vol. 7, No. 3, pp. 348-368, September 1981.